PROCEEDINGS, 48th Workshop on Geothermal Reservoir Engineering
Stanford University, Stanford, California, February 6-8, 2023
SGP-TR-224

Structural Assessment for Well Targeting in the Dieng Geothermal Field, Eastern Part of North Serayu Gea-Anticline

Iqbal Maratama, Taufik Al Amin, Siti Olivinia Yusra, Rizkhy Ridoh Alamsyah, Alfiady, Randy Wijaya Atmaja, Maxwell Wilmarth

PT Geo Dipa Energi, Jl. Akses Tol Soroja, Blok Sumakamanah Parungserab, No.22, Parungserab, Soreang, Bandung

Jacobs Indonesia, Talavera Office Park, 15th Floor, LetJen. TB. Simatupang Street, Kav. 22-26, Jakarta, DKI Jakarta

iqbal@geodipa.co.id

Keywords: structure, well targeting, permeability, Dieng, geothermal

ABSTRACT

Geologic structures are a primary target for drilling sweet spots in andesitic volcanic-arc hosted geothermal fields. This is due to the structures' (e.g., faults, breccia zones, fractured lithologic contacts) contribution of a zone of permeability in the reservoir. The data representing the structure on the surface and in the subsurface data have the potential to be connected. Surface data, such as lidar and resistivity can be useful for combining with subsurface well data. This data is integrated and analyzed to become an important parameter in the production and injection well targeting.

The Dieng Geothermal Field is located on the eastern part of North Serayu Gea-anticline formed by the southern Java subduction. This structural trend is inferred to control local volcanic activity such as Mount Sindoro and Sumbing, located in the SE of the field. The main structures that control the Dieng reservoir are shear fractures with NW-SE trend and extensional fractures trending W-E and N-S. Some of the N-W and W-E extensional fractures form normal faults. Faults which are caused by volcanic activities show W-E trend.

The focus of this study is to assess geologic structural data as the primary component for well targeting in a two-phase liquid dominated geothermal system. Surface data such as surface lineaments, quantitative surface structure analysis, and thermal manifestations are included in this study. Meanwhile, subsurface data such as MeQ, Gravity, well PTS data, Borehole Image Logs, and Loss zone data are utilized. The final outcome of this research is a structural level classification based on the relationship between structural data and the permeable zones in the reservoir, which may be utilized to develop the optimum strategy for well targeting.

1. INTRODUCTION

The Dieng Geothermal Field is located 26 km to the north of Wonosobo Regency and 110 km to the northwest of Yogyakarta City, Central Java Province, Indonesia. The field is situated within a volcanically active mountainous area on the eastern part of the North Serayu Gea-anticline range with a dominant northwest-southeast (NW-SE) structural trend, represented by the Sileri, Merdada, Sikidang, and Pakuwaja Craters. This trend is inferred to control volcanic activity given that Mount Sindoro and Sumbing, located in the SE of the field, also follow this trend. In the regional geological map the NW-SE trend also appears in the Tertiary rock distribution. In addition, results of structural mapping in 2013 indicate the major NW-SE structures are probably deeply penetrating and control the geothermal system. The Dieng geothermal reservoir consists of the northern Sileri area and southern Sikidang area, each with distinct reservoir properties. Resource evaluation indicates the Sileri area hosts a high-temperature, deep, two-phase, liquid-dominated geothermal system with neutral reservoir chemistry and high chloride and silica concentrations.

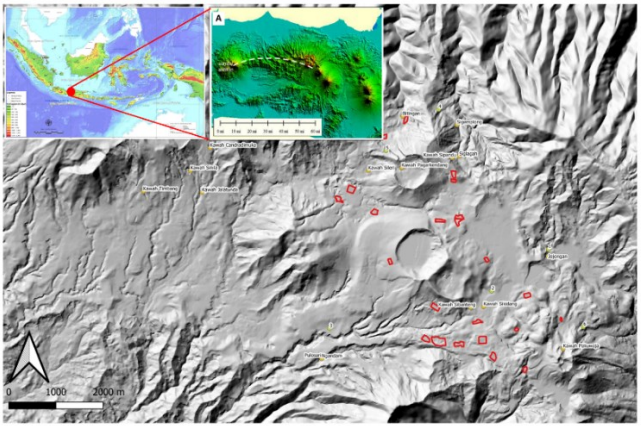

Figure 1: Dieng Geothermal Field located on the eastern part of North Serayu Gea-anticline

The result of geological mapping, which encompasses the Dieng Contract Area, has identified 23 lithology units. The analysis of K-Ar dating was conducted for eight lithology units (Boedihardi, 1991 on Resource Target Area Dieng, SPDEP Phase 1). However, in order to determine age for the rest of lithology units, relative age or comparison to the other lithology units are used. Based on relative age, lithologic units can be divided into two groups:

- Old volcanic products

Volcanic products with estimated age older than the Quaternary Period, i.e. Gajahmungkur, Prau (3.6 Ma), Reban, Sigemplong, Nagasari (2.99 Ma), and Jimat volcanic products. These volcanic products encompass the north and west area of the Dieng Field.

- Young volcanic products

Volcanic products estimated formed in the Quaternary Period, i.e. Bisma (2.53 Ma), Sidede, Sembungan, Pagerkandang (0.46 Ma), Sipandu, Pangonan (0.37 Ma), Merdada, Igir Binem, Prambanan, Watusumbul, Sikunir, Kendil (0.19 Ma), Pakuwaja (0.09 Ma), Seroja (0.07 Ma), Sikunang, and Alluvial units. These volcanic products encompass the center, southeast, and south of the Dieng Field.

The old volcanic products are predominantly comprised of pyroxene andesite, tuff breccia, and intercalated tuff- lapilli tuff. Andesite intrusions are also found in the outcrop of the Prau product, which are probably the same intrusions found in the well lithology (andesite complex). The young volcanic products also predominantly consist of tuff breccia, pyroxene andesite, biotite andesite, and intercalated tuff- lapilli tuff.

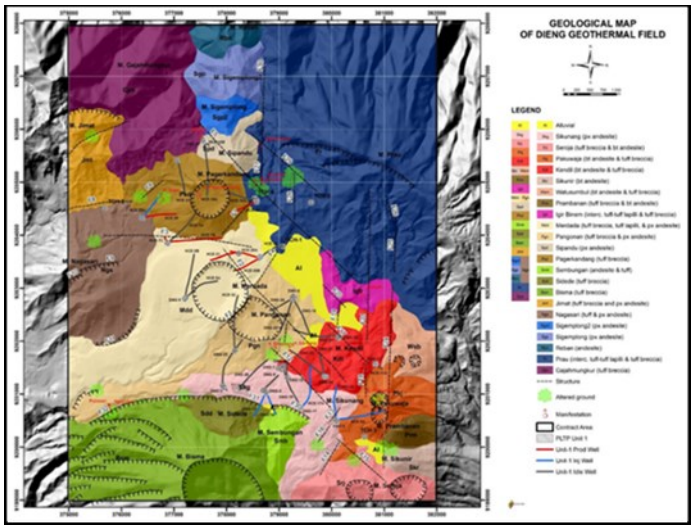

Figure 2: Geological map of Dieng Geothermal Field

Detailed geoscience surveys and drilling activities were carried out by two companies, Pertamina and Himpurna California Energy (HCE), beginning in 1975 and ending due to the economic crisis in 1998. During that period, 47 wells and five slim holes were drilled to confirm the potential of the field. The 47 wells are distributed across the field. However, several wells' data are incomplete, particularly in the Sikidang area.

2. METHODOLOGY AND DATA AVAILABILITY

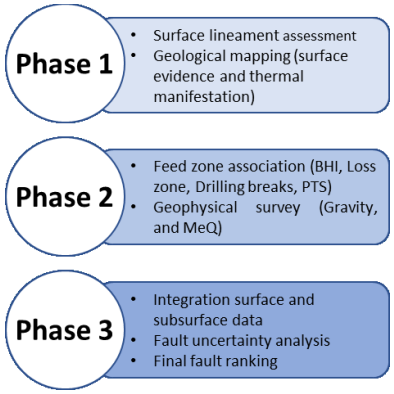

Figure 3: Fault and structure permeability assessment workflow

The major challenge in trying to perform a fault ranking or assessment is that there is little subsurface available data, and BHI data was only available when the most recent project began. Figure 2 shows a flowchart that is used to figure out the correlation between structure data and original permeability.

The initial investigation started with the interpretation of remote sensing data to determine the lineament based on the morphological alignment upon this surface of the visible color hue. Furthermore, field mapping was performed to determine the surface structure and manifestations that developed as an indication of surface structure development. The geometry of the fault is then analyzed and sorted based on data availability and its relationship to thermal features in the field. First rank faults can provide a high level of confidence over surface faults with good permeability.

Some BHI data from the subsurface is used to determine the subsurface structure, which is supported by drilling data such as loss zones, drilling breaks, and PTS data during completion, which can be a reliable data benchmark to determine data relationships. Geophysics data is also used in the assessment structure as one of the assessments.

The compiled and analyzed surface and subsurface data will be integrated and correlated to determine the relationship between structure and permeability as a basis for determining structural assessments related to permeability. The end result of this research is fault ranking as a reference for determining the next drilling target with a high ranking or a high level of confidence and productivity.

Details	Tools	Type
Surface Data	Lineament	Soft
	Surface structure	Hard
	Manifestations	Hard
Subsurface Data	Borehole Image	Hard
	Loss zone	Hard
	Drilling break	Hard
	PTS	Hard
	MT	Soft
	Gravity	Soft
	MeQ	Soft

Figure 4: Data availability

3. TECTONIC AND SURFACE STRUCTURE

The regional tectonic setting of Dieng which located in Java Island, situated in the central part of Sunda volcanic arc that has formed due to subduction of northward moving oceanic crust Indo-Australia beneath Eurasia plate extended from Andaman Island to the east through Sumatra, Java, Bali until Flores Island (Hamilton, 1978). The thickness of Eurasia plate beneath Sumatra to Java is about 20 to 30 km and is around 18 km close to Bali. The subducting plate is an oceanic plate with the age from ~80 Ma to ~130 Ma ranges from Sumatra to Java. The subduction rate of the Indo Australian plate beneath Eurasia is 6 to 7 cm/year.

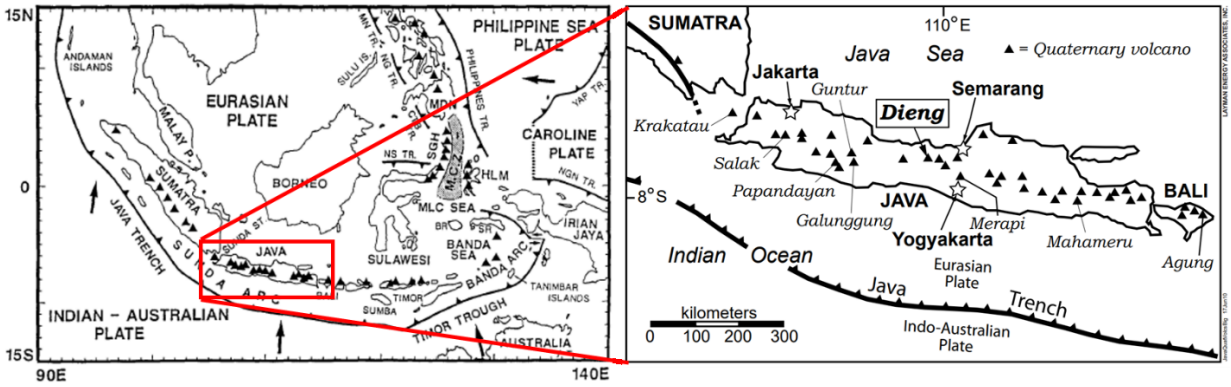

Figure 5: Regional tectonic framework (Left) and Current map regional study (Right). (Layman, 2002 and Harijoko, 2010)

3.1 Remote Sensing

Statistical analysis of 1,651 lineaments reveals that the dominant lineament is in the east-west direction. The alignments that stand out in the northern part, which is covered by old lithological units (Gajah Mungkur, Jimat, Prahu, Nagasari, Reban, Sigemplong 1 and Sigemplong 2), are those trending northeast-southwest (NE-SW) and northwest-southeast (NW-SE) as representations of the oblique shear joints that develop in the North Serayu anticline.

The east-west direction (E-W) dominates the lineaments that develop in the central to southern part of the study area, which is filled with young volcanism (Pagerkandang, Merdada, Pangonan, Alluvial, Kendil, Sikunang, Pakuwaja, Seroja, Prambanan, Watusumbul, and Sikunir units).

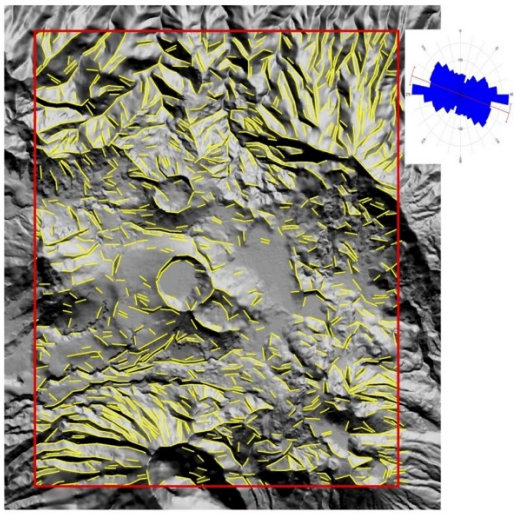

Figure 6: Lineament of study area from Remote sensing

3.2 Surface Structures and Manifestations

There are 238 extension joints and 158 shear joints based on the data. The shear joint maxima are oriented NE-SW and NW-SE, while the extension joint maxima are oriented N-S and E-W. Oblique shear joints are formed by the compression forces of the North Serayu geanticline. Spreading of the extensional zones at the anticline's crests and wings results in extension joints. There are several joints in the structural analyses that are in accordance with the delineation of the remote sensing lineament, showing that there is an appropriate trend between the remote sensing delineation and direct calculation of the structure on the surface.

The Sileri area hosts numerous geothermal features including hot springs, craters, lakes, solfatara, altered ground, and mud pools. The presence of multiple manifestations in the study area indicates a developing structure that causes multiple manifestations to develop.

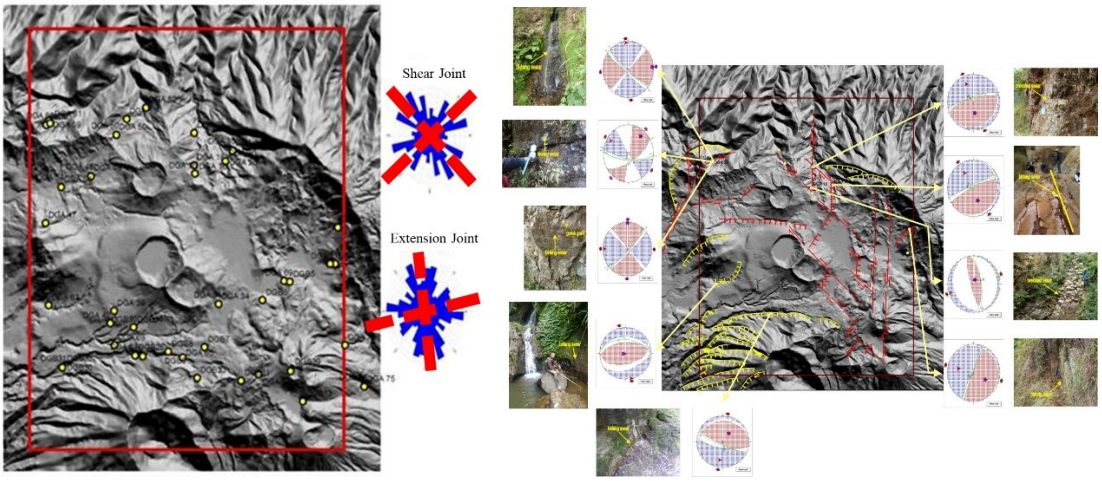

Figure 7: Statistic analytic and measurement surface structures

3.3 Surface Structures Ranking

Although several surface fault cases do not directly represent subsurface conditions, ranking surface structures based on their appearance can be an illustration of the trend of structures developing in the study area due to tectonics or volcanism. A surface fault ranking is calculated using several parameters. A structure with a high rating has a lot of surfaces observed evidence, whereas a structure with a lower ranking has less surface evidence. The ranking of these surface structures begins with digital and manual surface lineament data, followed by concrete evidence of the presence of structures on the surface and additional manifestation data surrounding these structures.

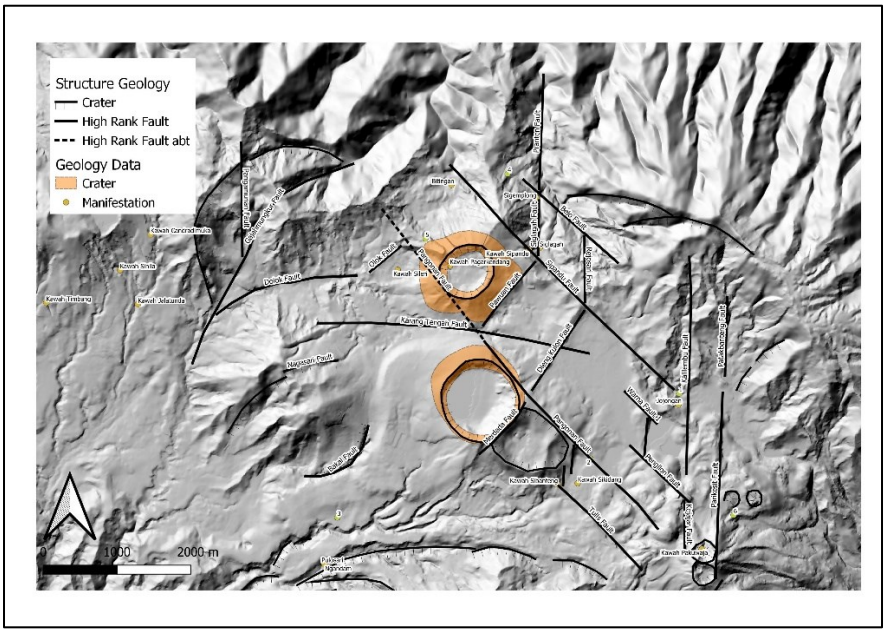

Fault Name	Fault ID	Lineament								Thermal Manifestation Occurrence		Surface Fault Existance
		Surface Lineament (GDE)		Manual Extraction		Digital Extraction		Surface Evidence				
Karang Tengah Fault	F3	High	3	Mid	2	Mid	1	No	0	No	0	6
Pangonan Fault	F2	High	3	Mid	2	Mid	1	No	0	No	0	6
Sipandu Fault	F5	High	3	High	3	High	2	No	0	Yes	3	11
Merdada Fault	F1	Mid	2	High	3	High	2	No	0	No	0	7
Dieng Kulon Fault	F4	Mid	2	High	3	Mid	1	No	0	No	0	6
Pawuan Fault	F7	No	0	Low	1	Mid	1	No	0	No	0	2
Nagasari Fault	F9	Mid	2	High	3	High	2	No	0	No	0	7
Bakal Fault	F11	Mid	2	High	3	High	2	Yes	1	No	0	8
Siglagah Fault	F27	High	3	High	3	High	2	Yes	1	Yes	3	12
Rejosari Fault	F28	High	3	High	3	High	2	No	0	No	0	8

Crater Name	Lineament								Thermal Manifestation Occurrence		Crater Existance
	Surface Lineament (GDE)		Manual Extraction		Digital Extraction		Surface Evidence				
Merdada Crater	High	3	High	3	High	2	No	0	Yes	3	11
Pagarkendang Crater	High	3	High	3	High	2	No	0	Yes	3	11

Figure 8: Surface fault ranking

4. SUBSURFACE PERMEABILITY

4.1 Feed Zone PTS and Loss Zone

Mainly data for interpreting subsurface permeability is from feed zones location. Feed zones data from existing well is not sufficient due to obstruction during logging surveys in the wells. Based on current drilling project in Dieng, loss zones and bore hole image data give permeability indication in resevoir. Completion test was held to confirm the location and contribution of feed zones in each wells. Distribution of feed zones data in Dieng based on existing and current drilling project are spread in both of shallow and deep reservoir zones. These feed zones have a quantitative value that can be proven data for determining permeability related to surface structures.The feed zones location in Dieng ranging from 1200 mASL to -800 mASL. However, in general, the inflow feed zone is shallower than the outflow feed zone. It is evident from these data that there is a discontinuity zone between the shallow and deeper reservoirs.

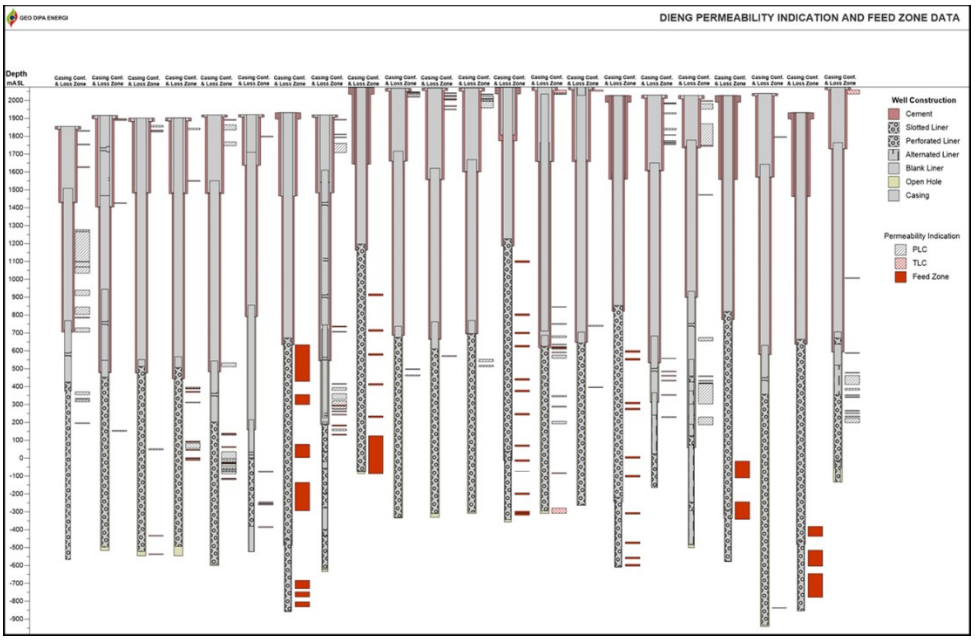

Figure 9: Cross section of vertical PTS feed zone and Loss Zone distribution

4.2 Gravity, and MeQ

Gravity and MeQ can identify subsurface structures based on current data trends. Gravity is an indirect method whose results are unaffected by geothermal activity, and it can be used to delineate subsurface geological structures by comparing density values. Meanwhile, MeQ data is geophysical data used to calculate subsurface micro earthquake events. The distribution and clusters of existing micro earthquake events can be seen in this data. These data support several surface structures that correlate with indications of structures beneath the surface. Structures that are related to gravity data include the Karangtengah Fault, Pawuan Fault, and Merdada Fault.

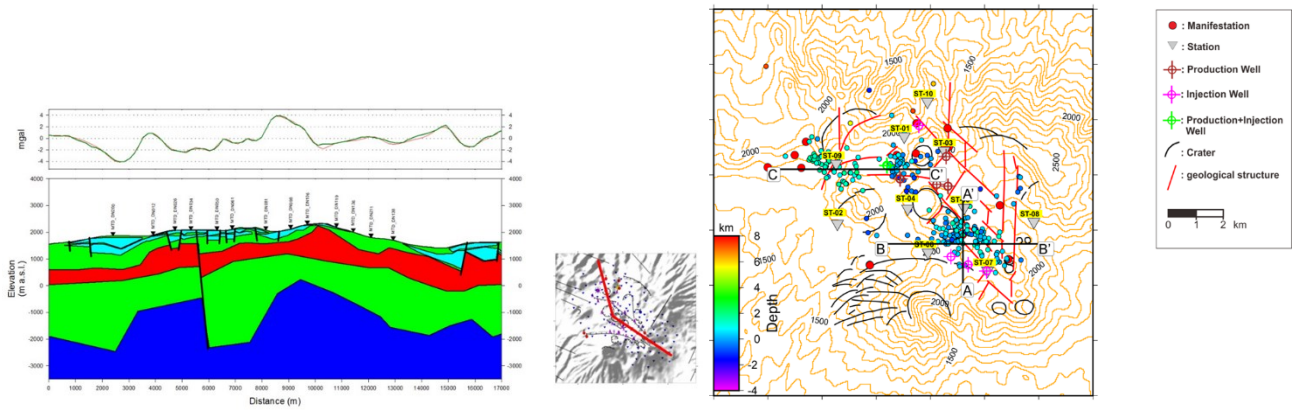

Figure 10: Cross section of Gravity and distribution of MeQ data

4.3 Borehole Image

The data used in this study came from SLR-J and SLR-Q consisting of wireline log (borehole image logs), pressure and temperature (PT) survey, and drilling data. Additionally, compressional and shear wave slowness from SLR-Q1 is also used to analyse mechanical properties of formation due to the absent of this data in SLR-J and SLR-Q. Summary of the data in SLR-J and SLR-Q can be seen in Figure 11.

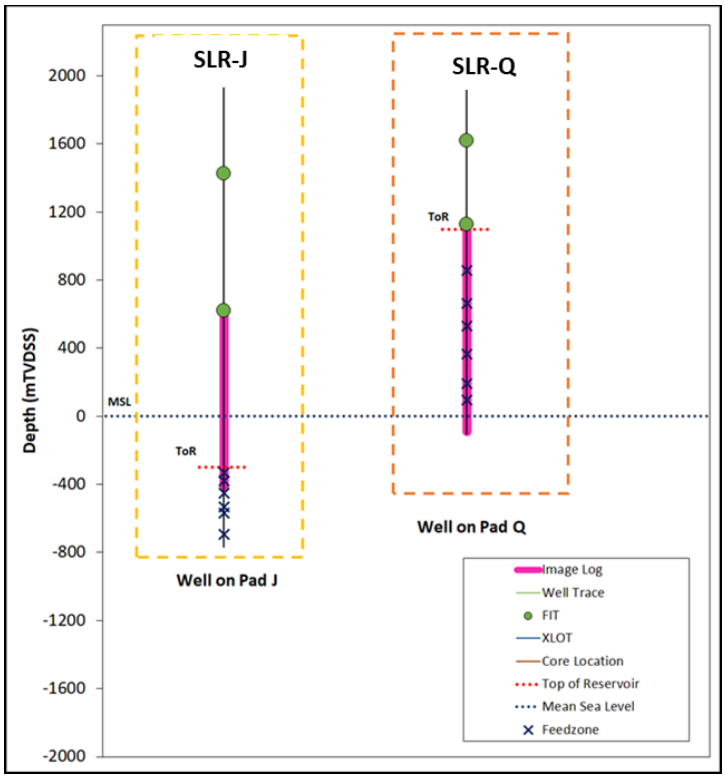

Figure 11: Data availability to conduct geomechanics analysis.

One dimensional geomechanics model consist of in-situ stress (magnitudes and orientations), pore pressures, formation elastic and strength properties, which were calibrated with formation integrity test (FIT), wellbore failures (drilling induced tensile fractures), and drilling data is built to understand the stress configuration and its implication on fracture permeability. Pore pressure is directly used from given PT measurement. Vertical stress is derived from density-sonic log correlation using Gardner et. al. (1974). Horizontal minimum stress is calculated with Matthews, W. R. and Kelly, J. (1967) equation which later validated by FIT data. The used of FIT data might present some uncertainty since horizontal minimum stress is better to be validated with instantaneous shut in pressure (ISIP) from extended leak-off test (XLOT) data. Maximum horizontal stress is obtained from the wellbore failure observations (drilling induced tensile fracture) hence can be calculated empirically according to Zoback (2007) with the given value of friction coefficient, pore pressure, horizontal minimum stress, and vertical stress. Due to the inclined wellbore geometry which means no principal stress parallel to the wellbore axis, determination of horizontal maximum stress azimuth needs to be calculated rigorously using modelling of stress around wellbore wall. Detailed method on calculating stress of inclined wellbore already demonstrated by Barton et al. (1998), Peska and Zoback (1995), and Hiramatsu, Y., and Oka, Y. (1962, 1968).

Figure 12 summarizes the stress profile of both SLR-J and SLR-Q. Pressure data come from PT survey while horizontal minimum stress is calculated empirically using Matthews, W. R. and Kelly, J. (1967) which then validated by FIT data. Overburden stress is calculated by integrating the density value from sonic-density correlation on nearby SLR-Q1 well. Horizontal maximum stress magnitude is obtained empirically and validated with drilling induced tensile fractures occurrence in the wellbore. Due to the absent of compressional and shear wave slowness in both wells, mechanical properties such as unconfined compressive strength (UCS), tensile strength (T0), internal friction angle, and porosity is obtained from sonic derivation in the nearby SLR-Q1. Figure 12 shows strike slip to thrust stress regime domain which means horizontal maximum stress act as the maximum principal stress and horizontal minimum stress act as the least principal stress.

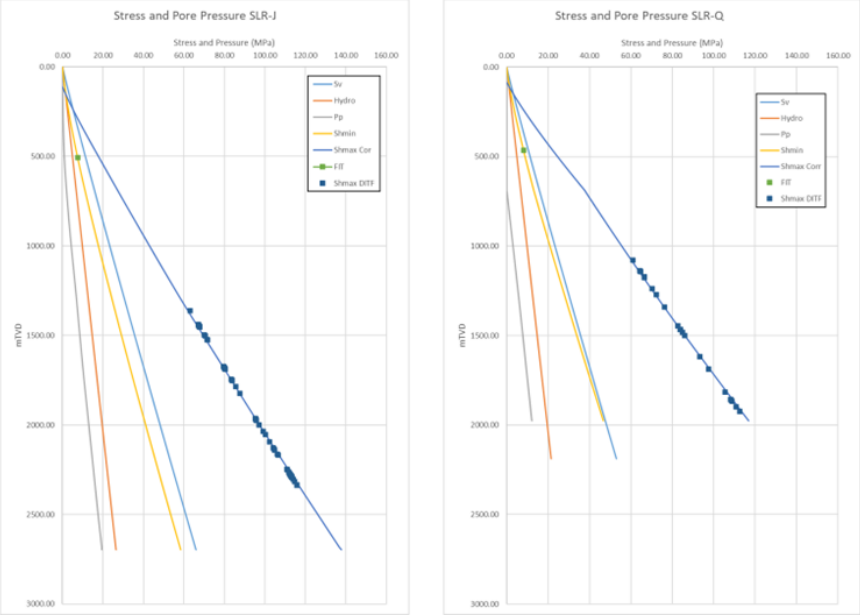

Figure 12: Stress profile on SLR-J and SLR-Q generally shows strike-slip to thrust stress regime, indicated by the elevated Shmin value which almost similar with Sv (vertical stress).

Mechanical properties on SLR-Q1 (Figure 13) shows competent rock having quite high UCS value around 165-216 MPa which is included in very strong rock according to Attewell and Farmer (1976) utilizing dynamic estimates with compressional and shear sonic as input calculation. The average friction angle of 55 degrees also supports a competent rock type. This value is utilized as consideration to put reasonable mechanical properties value to estimate the horizontal maximum stress.

UCS (Mpa)		*Tensile Strength (Mpa)*		*Porosity (%)*		*Int Fric Angle (deg)*	
Mean	193.56	Mean	19.36	Mean	2.81	Mean	54.85
Standard Error	0.13	Standard Error	0.01	Standard Error	0.02	Standard Error	0.02
Median	192.31	Median	19.23	Median	2.75	Median	54.91
Mode	208.43	Mode	20.84	Mode	1.05	Mode	56.70
Standard Deviation	10.07	Standard Deviation	1.01	Standard Deviation	1.42	Standard Deviation	1.49
Sample Variance	101.42	Sample Variance	1.01	Sample Variance	2.00	Sample Variance	2.21
Kurtosis	-0.51	Kurtosis	-0.51	Kurtosis	1.60	Kurtosis	1.60
Skewness	-0.01	Skewness	-0.01	Skewness	0.96	Skewness	-0.96
Range	51.14	Range	5.11	Range	8.48	Range	8.91
Minimum	165.60	Minimum	16.56	Minimum	0.41	Minimum	48.46
Maximum	216.74	Maximum	21.67	Maximum	8.89	Maximum	57.37
Sum	1118573.96	Sum	111857.40	Sum	16216.74	Sum	316998.62
Count	5779.00	Count	5779.00	Count	5779.00	Count	5779.00

Figure 13: Summary statistics of strength properties in SLQ-Q-31A from compressional and shearwave slowness derivation.

Stress concentration around wellbore evaluation in both SLR-J and SLR-Q in specific depth interval where drilling induced tensile fracture is observed generally shows NNE-SSW to NE-SW. In vertical well, this azimuth will imply directly as the horizontal maximum stress azimuth. Using more rigorous method, estimation of the maximum horizontal stress direction using stress concentration around wellbore wall modelling shows azimuth direction of N15E and N28E for SLR-J and SLR-Q, respectively. These values generally follow the far-field stress in Java due to Indo-Australian plate subducting beneath Eurasian plate. Because of the inclined wellbore geometry, it appears a 3 degrees clockwise rotation between the maximum horizontal stress direction from modelling and the drilling induced tensile fracture direction observed in the image log. The 3 degrees clockwise shift is due to the inclined wellbore geometry resulting in slight changes in stress concentration around wellbore wall. The rotation is considered to be insignificant added with no shifting in SLR-J which means tensile fracture direction already confirm the azimuth of horizontal maximum stress.

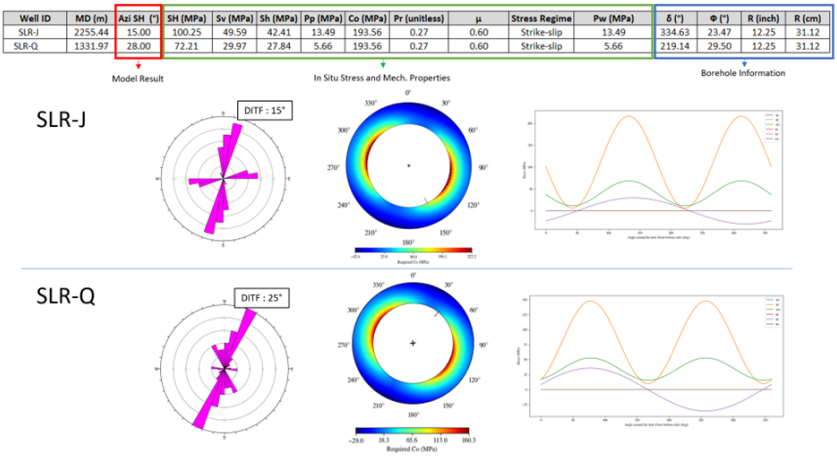

Figure 14: Modeling of stress concentration

Modeling of stress concentration around wellbore wall on SLR-J and SLR-Q to obtain the orientation of maximum horizontal stress. Drilling-induced tensile fracture (DITF) is interpreted from image log data. Note: azi SH = SHmax azimuth, Co = rock strength, μ = coefficient of internal friction, v = Poisson'sratio, δ = borehole azimuth and Φ = inclination.

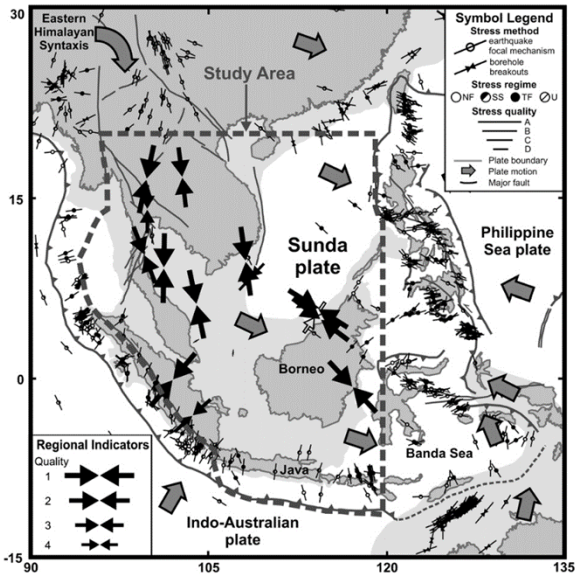

Figure 15: Mean maximum horizontal compression stress azimuth in Java (Tingay et. Al., 2010).

These models imply the strike slip stress regime to thrust stress regime currently work in Dieng field. The model suggest structure with strike around 30 degrees from the azimuth of horizontal maximum stress, NNW-SSE and NE-SW to be critically stressed hence promote good structural permeability.

5. FINAL FAULT RANKING

Permeability and subsurface structure indications do not always correlate with surface structure indications. To obtain good and comprehensive information, there is a need for integration and data correlation between surface structure and subsurface permeability. This data can be analyzed and correlated to provide more information about the geometry of the structure and the extension of the proven zone in geothermal systems. This analysis can yield both proven and less proven structural sequences. Structures with good values, on the other hand, are not always bad, because good structural values are supported by subsurface data and number data in the structure zone, and the sequence of structures can change at any time due to the availability of subsurface data and drilling data. However, ranking this structure can improve the probability of success against the target to be drilled, so it is critical for well targeting in the next drilling operation.

Surface structures with a high ranking, such as the Siglagah, Sipandu, and Rejosari structures, have not been proven to have a good ranking, according to the current interpretation, because they have never been drilled towards these structures. Meanwhile, structures that

are not very good in terms of surface structure ranking, such as the Karangtengah, Pangonan, Pawuan, and Merdada structures, have a high permeability ranking level due to good and proven subsurface data. What makes the Merdada and Pagerkandang craters slightly unique is that their surface structure and permeability rank in the good-medium range.

Fault Name	Fault ID	Feed Zone Association						BHI	Drilling Breaks		Geophysics Survey (SPDEP)				Permeability	Permeability Ranking	Surface Fault ranking
		PLC		TLC		PTS					MT		Gravity				
Karang Tengah Fault	F3	Yes	5	Yes	6	Yes	6	5	Yes	1	Yes	1	Yes	1	25	1	5
Pangonan Fault	F2	Yes	2	Yes	3	Yes	5		Yes	1	Yes	1	No	0	12	2	5
Sipandu Fault	F5										Yes	1	No	0	1	5	2
Merdada Fault	F1	No	2	No	3	Yes	3		Yes	1	Yes	1	Yes	1	11	3	4
Dieng Kulon Fault	F4										Yes	1	No	0	1	5	5
Pawuan Fault	F7	Yes	2	Yes	3	Yes	3		Yes	1	Yes	1	Yes	1	11	3	6
Nagasari Fault	F9														0	6	4
Bakal Fault	F11														0	6	3
Siglagah Fault	F27														0	6	1
Rejosari Fault	F28														0	6	3

Crater Name	Feed Zone Association						BHI	Drilling Breaks		Geophysics Survey (SPDEP)				Permeability	Permeability Ranking	Surface Fault ranking
	PLC		TLC		PTS					MT		Gravity				
Merdada Crater	Yes	3	Yes	5	Yes	4		Yes	1					8	4	2
Pagarkendang Crater	Yes	2	Yes	3	Yes	4	5	Yes	1					12	2	2

Figure 16: Final structure ranking of (Sileri) Dieng geothermal system

CONCLUSION

Several surface structures are related to the PTS feed zone data's subsurface permeability. This is a good finding for increasing confidence in subsurface permeability to surface targets. The Karangtengah fault, which has strike slip fault movement based on borehole image data, is the best geological structure in terms of permeability. Aside from that, the Pangonan, Pawuan, and Merdada faults have high subsurface permeability and can be used as drilling targets. Merdada and Pagerkandang craters are also candidates for further expansion. Other structures may not have made a significant contribution to subsurface permeability up to this point due to a lack of data surrounding these structures.

There is a discontinuity area that separates the permeability of the shallow reservoir from the permeability of the deep reservoir for the distribution of vertical feed zones from existing wells. This discontinuity area is located between -300 to -400 mASL. It is still possible to develop other methods and additional data from the feed zone, drilling data, and more well data from this study in order to gain a better understanding of the subsurface structure.

REFERENCES

Attewell, P. B., and Farmer, I. W. (1976): Principles of Engineering Geology, London: Chapman and Hall.

Barton, C. A., Castillo, D. A., Moos, D., Peska, P., and Zoback, M. D. (1998): Characterising the full stress tensor based on observations of drilling-induced wellbore failures in vertical and inclined boreholes leading to improved wellbore stability and permeability prediction, The APPEA Journal, 38(1), 466–487.

Dieng Subsurface Team: Detail Well Targeting Dieng, SPDEP Phase 2, Internal Report of Geodipa (2021).

Dieng Subsurface Team.: Dieng Well Prognosis and Resources Risk & Uncertainty Mitigation Plan, SPDEP Phase 3, Internal Report of Geodipa (2021).

Harijoko, Agung, et al.: Long-Term Volcanic Evolution Surrounding Dieng Geothermal Area, Indonesia, Proceedings World Geothermal Congress, (2010)

Hiramatsu, Y., and Oka, Y. (1962): Stress around a shaft or level excavated in ground with a three-dimensional stress state, Memoirs of the Faculty of Engineering, Kyoto University, 24 (1962),.

Hiramatsu, Y., and Oka, Y. (1968): Determination of the stress in rock unaffected by boreholes or drifts, from measured strains or deformations, International Journal of Rock Mechanics and MiningSciences & Geomechanics Abstracts, 5(4), 337–353.

Layman, B Erik., Irzarwadi Agus., and Samsudin Warsa.: The Dieng Geothermal Resource, Central Java, Indonesia, Geothermal Resources Council Transactions, (2002), Vol. 26.

Matthews, W. R. and Kelly, J. (1967): How to predict formation pressure and fracture gradient, Oil and Gas Journal, February, 92–106.

Peska, P., and Zoback, M. D. (1995): Compressive and tensile failure of inclined well bores and determination of in situ stress and rock strength, Journal of Geophysical Research, 100(B7).

Resources and Facility Team.: Resource Target Area Dieng, SPDEP Phase 1, Internal Report of Geodipa (2020).

Tingay, M., Morley, C., King, R., Hillis, R., Coblentz, D., and Hall, R. (2010): Present-day stress field of Southeast Asia, Tectonophysics, 482(1–4), 92–104.

Zoback, M. D. (2007): Reservoir geomechanics, Cambridge University Press.